THE JOURNAL OF PHYSICAL CHEMISTRY B

Article

pubs.acs.org/JPCB

Effects of Hydrogen Bonding on Internal Conversion of GFP-like Chromophores. I. The *para*-Amino Systems

Guan-Jhih Huang,[†] Chi-Wen Cheng,[‡] Hung-Yu Hsu,[‡] Ch. Prabhakar,[†] Yuan-Pern Lee,*[,‡,§] Eric Wei-Guang Diau,*[,‡] and Jye-Shane Yang*[,†]

[†]Department of Chemistry, National Taiwan University, Taipei 10617, Taiwan

[‡]Department of Applied Chemistry and Institute of Molecular Science, National Chiao Tung University, Hsinchu 30010, Taiwan

[§]Institute of Atomic and Molecular Sciences, Academia Sinica, Taipei 10617, Taiwan

Supporting Information

ABSTRACT: To understand the effects of solvent−solute hydrogen bonding (SSHB) on the excited-state dynamics of two GFP-like chromophores, *p*-ABDI and *p*-CFABDI, we have determined the quantum yields for fluorescence (Φ_f) and the isomerization $Z \rightarrow E$ (Φ_{ZE}) and the femtosecond fluorescence and transient infrared absorption in selected solvents. The behavior that $\Phi_{ZE} \cong 0.50$ in aprotic solvents, such as CH_3CN, indicates that the E−Z photoisomerization adopts a one-bond-flip mechanism through the torsion of the exocyclic C═C bond (the τ torsion) to form a perpendicular species (τ ~90°) in the singlet excited state followed by internal conversion (IC) to the ground state and partition to form the E and Z isomers with equal probabilities. The observed Φ_{ZE} decreased from 0.50 to 0.15−0.28 when CH_3CN was replaced with the protic solvents CH_3OH and CF_3CH_2OH. In conjunction with the solvent-independent rapid (<1 ps) kinetics for the fluorescence decay and the solvent-dependent slow (7−20 ps) kinetics for the ground-state recovery, we conclude that the SSHB modifies the potential energy surface for the τ torsion in a way that the IC occurs also for the twisted intermediates with a τ-torsion angle smaller than 90°, which favors the formation of the Z isomers. The possibility of IC induced by torsion of the exocyclic C−C bond (the φ torsion) is also considered but excluded.

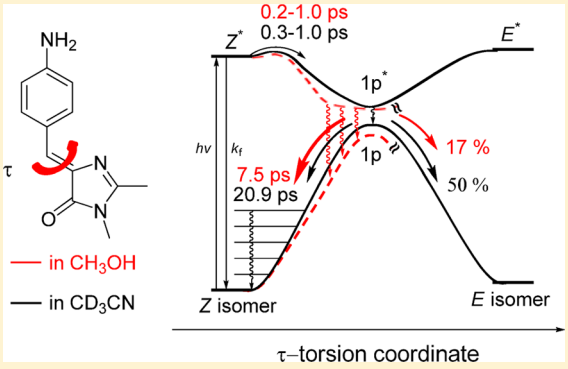

INTRODUCTION

The great utility of green fluorescent protein (GFP) and many of its colorful mutants as biological markers[1] renders the understanding of their structure−fluorescence property relationship a fundamentally important issue. An unsettled question in this context is the origin of fluorescence quenching (fluorescence quantum yield $\Phi_f < 10^{-3}$) of the chromophore, *p*-hydoxybenzylidenedimethylimidazolinone (*p*-HBDI, Chart 1), when it is detached from the protein matrix (the β-barrel).[2] The observation[2] of the fluorescence recovery ($\Phi_f \sim 0.8$) for *p*-HBDI in solvent glasses at 77 K has directed the discussion to large amplitude torsional motions of either the exocyclic C—C (φ) or the C═C (τ) bond (Chart 1).[2−6] However, the small dependence of the fluorescence decay rates on solvent viscosity was ascribed to a volume-conserving hula twist, namely, a concerted torsion of both the C—C and C═C bonds.[7] Recently, we discovered that the solute−solvent hydrogen bonding (SSHB) plays an important role in the deactivation of excited *p*-HBDI, based on the observation of a significantly decreased quantum efficiency (Φ_{ZE}) of the $Z \rightarrow E$ photoisomerization when a protic solvent replaced an aprotic solvent of similar polarity (e.g., CH_3OH vs CH_3CN).[8] Because the excited state dynamics of the GFP chromophore in bulk solutions are complicated, further investigation is required to attain a satisfactory understanding of this topic.

A useful approach toward the elucidation of the excited-state dynamics of the GFP chromophore is through comparison of structurally related model compounds. For example, *p*-ABDI, the *para*-amino analogue of *p*-HBDI, possesses an electronic

Chart 1

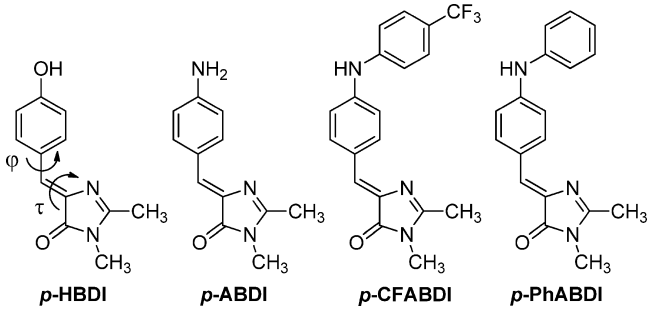

Received: September 20, 2012
Revised: December 17, 2012
Published: January 24, 2013

character between the neutral and anionic *p*-HBDI but has decay dynamics free from the complication of excited-state proton transfer (ESPT) of the phenol group. Another simplification of decay dynamics for *p*-ABDI vs *p*-HBDI is the enhanced thermal stability of its *E* isomer.[8] Through the N-aryl substituent effect[9] on the fluorescence enhancement, the interplay between Φ_{ZE} and Φ_f in different solvents can be readily analyzed for the N-aryl substituted derivatives of *p*-ABDI (e.g., *p*-PhABDI). Our previous work on *p*-ABDI, *p*-PhABDI, and related chromophores indicated that the SSHB interactions might couple to the channel of τ-torsion-induced internal conversion (IC) in view of its nonparallel influence in Φ_f and Φ_{ZE}, in which Φ_{ZE} but not Φ_f is sensitive to solvent proticity.[8,9]

To characterize further the excited state dynamics of these GFP-like chromophores, we measured femtosecond fluorescence up-conversion and time-resolved infrared (TRIR) spectra of *p*-ABDI and *p*-CFABDI in solutions. Compound *p*-CFABDI is expected to display fluorescence more intense than that of *p*-ABDI because of the N-aryl substituent effect.[9,10] The trifluoromethyl group in *p*-CFABDI is expected to decrease the ability of the amino group to donate electrons, so that the propensity to form a twisted intramolecular charge-transfer (TICT)[11,12] state by twisting either the phenyl-amino C−N bond or the exocyclic C−C bond (i.e., φ torsion) would be further reduced as compared to *p*-ABDI. Therefore, *p*-CFABDI would be a good reference for the discussion of the excited-state decay mechanism of *p*-ABDI. The results reported herein show that the SSHB fastens the recovery of the ground state but has a negligible influence on the fluorescence quenching for both *p*-ABDI and *p*-CFABDI. These observations are interpreted with the one-bond-flip (OBF) mechanism, in which the potential energy surface (PES) for the τ torsion is perturbed by SSHB so that partition of the τ-twisted intermediates to the *Z* isomers is more favorable than that to the *E* isomers.

EXPERIMENTAL SECTION

Steady-State Spectra. Infrared absorption spectra of the samples in their steady state were recorded with a Fourier-transform IR spectrometer (VERTEX-V80, Bruker) equipped with a KBr beam splitter and a photovoltaic Hg/Cd/Te detector (77 K) to cover the spectral range 770−8000 cm^{-1}. Typically, 100 scans at resolution 4 cm^{-1} were recorded in the experiment. Absorption of the solvent, measured separately using the pure solvent, was removed from the spectrum of the sample solution.

Ultraviolet−visible (UV−vis) absorption spectra of the samples, placed in a cuvette of path length 1.0 cm, were recorded with a double beam spectrometer (Cary 300, Varian) at a resolution of 1 nm.

Fluorescence spectra were recorded with a PTI Quanta-Master C-60 or an Edinburgh FLS920 spectrometer and corrected for the response of the detector. Solutions of anthracene (10^{-5} M in hexane) and quinine sulfate (0.5 M in sulfuric acid solution) served as standards (Φ_f = 0.27 for anthracene[13] and Φ_f = 0.55 for quinine sulfate[14]) for the determinations of the fluorescence quantum yields of compounds under N_2-outgassed solutions with correction for the refractive index of the solvent. An error of ∼10% is estimated for the fluorescence quantum yields.

Time-Resolved Fluorescence. The fluorescence decay was recorded with an optically gated (up-conversion) system (FOG100, CDP), which has been described elsewhere.[15] Briefly, the femtosecond laser system (Mira 900D, Coherent) generated light pulses at 800 nm of duration ∼160 fs at a repetition rate of 76 MHz. The laser pulses were frequency-doubled to generate pump pulses at 400 nm. The residual of the 800 nm pulse served as an optical gate. The intensity of the pump beam was appropriately attenuated with a neutral density filter to 0.4 nJ; this pulse was focused onto a rotating cell containing the sample solution with the length of optical path of 1 mm. The fluorescence emission was collected with two parabolic mirrors and focused onto a crystal (BBO, type I); the gate pulse was also focused onto the BBO crystal for sum-frequency generation (SFG). This SFG signal was collected with a lens and dispersed with a monochromator (DH10, Jobin Yvon) before being detected with a photomultiplier (R1527P, Hamamatsu) in the computer-controlled photon-counting system. On varying the temporal delay between the excitation and the gate pulses via a stepping translational stage, we obtained the temporal profile of fluorescence. The polarization between pump and probe pulses was fixed at the magic angle 54.7°. The sample was prepared in CH_3OH, CD_3OD, and CD_3CN (concentration 4.9−7.4 μmol L^{-1}) and outgassed prior to use.

Time-Resolved Infrared (TRIR) Absorption. The femtosecond transient IR absorption was recorded with a pump−probe method.[16] The laser pulses were generated with a regenerative amplifier (SPTF-100F-1K-XP, Spectra Physics) seeded with a mode-locked Ti:sapphire laser system (Mai Tai Sp, Spectra Physics) and pumped with a Nd:YLF laser (Empower 30, Spectra Physics, 1 kHz). This system produces pulses at 800 nm of duration ∼100 fs and average energy 4.0 mJ $pulse^{-1}$. This output pulse was split into three parts with a ratio of 40:40:20. The less intense (20%) beam served to generate a pump beam at 400 nm by second harmonic generation. The energy of this pump pulse was attenuated with a neutral density filter to 1−2 μJ and focused onto a sample cell containing the solution; the cell has two CaF_2 windows and a Teflon spacer (thickness 100 μm). One intense (40%) beam was directed into an optical parametric amplifier (TOPAS-C, Light Conversion) to generate tunable near-IR pulses of signal and idler beams, followed by difference frequency generation in an $AgGaS_2$ crystal to generate the mid-IR probe beam tunable from 5.7 to 6.6 μm. This IR probe pulse was split into two equal parts for use as sample and reference beams; the sample probe beam spatially overlaps with the pump beam. The optical delay between the pump and probe beams was achieved with a stepping translational stage (SGSP(MS)26-200(X), Sigma Koki). The sample cell was rotated with a speed of ∼3000° s^{-1} so that each pump pulse excited a fresh sample region. After passing through the sample, the two IR probe beams were collimated and dispersed with a spectrograph (Micro HR, Jobin-Yvon Horiba) and detected separately with a 2×32-element Hg/Cd/Te array detector (IR-6416, Infrared Systems Development Corp.) to yield spectra of resolution 3−4 cm^{-1}. Every other pump pulse was blocked with a synchronized chopper (MC1000A, Thorlabs) operated at 500 Hz; the change in absorbance (ΔA) was calculated from the intensities of sequential probe pulses with and without pumping. To decrease the noise further, ΔA recorded with the reference beam (no pumping) was subtracted from that recorded with the sample beam. The instrument response function (IRF) and the zero time delay were determined with a thin Si wafer, which has instantaneous mid-IR absorption upon excitation at 400 nm.

dx.doi.org/10.1021/jp3093379 | J. Phys. Chem. B 2013, 117, 2695−2704

The IRF was characterized with a Gaussian function of full width at half-maximum (fwhm) of ~300 fs. The polarization between pump and probe pulses was fixed at the magic angle 54.7°. The sample was prepared in CH_3OH, CD_3OD, and CD_3CN (concentration 4.9−7.4 mmol L^{-1}) and outgassed prior to use.

Photoisomerization. Quantum yields of the $Z \rightarrow E$ photoisomerization (Φ_{ZE}) were measured for optically dense outgassed solutions (3×10^{-3} M) at 350 nm with a Xe arc lamp (75 W) and a monochromator. *trans*-4-(*N*-Phenylamino)-stilbene served as a reference standard (Φ_{tc} = 0.34 in CH_2Cl_2).[12] The extent of photoisomerization (<10% conversion) was determined with HPLC analysis (Waters 600 Controller and 2998 photodiode array detector probed at 290 nm, Thermo APS-2 Hypersil, hexane and ethyl acetate mixed solvent as eluent, and 1,4-dioctyloxybenzene of 1×10^{-3} M as internal standard) without correction for back reaction. The reproducibility error was <10% of the average. The isomerization quantum yield is determined on the basis of the following equation:

$$\frac{C_r \times V_r \times P_r}{\Phi_{tc} \times t_r} = \frac{C_s \times V_s \times P_s}{\Phi_{ZE} \times t_s}$$

where C is the concentration of substrates, V is the volume of solutions, P is the amount (%) of substrate that is converted to the *cis* (for the stilbene standard) or E isomer (for *p*-ABDIs) after irradiation, t is the irradiation time (s), and the subscripts r and s denote the reference standard and the substrates *p*-ABDIs, respectively. In all cases, the HPLC traces show a single product formation, corresponding to the *cis* or E isomer, as confirmed by ^{1}H NMR (Figure S1, Supporting Information). The P values were determined on the basis of the consumption of the substrates (i.e., the disappearance of the corresponding *trans* and Z isomer) according to the changes in HPLC integrated peak intensity relative to the internal standard.

Calculations. All calculations were performed with the software Gaussian 09.[17] The electronic ground- and excited-state geometry optimizations adopted the density functional theory (DFT) and time-dependent density functional theory (TDDFT) methods, respectively. Becke's three-parameter hybrid exchange functional and the Lee−Yang−Parr correlation functional (B3LYP) were utilized in the calculation[18] with a 6-31G* basis set. Vibrational frequencies were evaluated for the optimized geometries in the gas phase at the same level to ensure that the structure obtained was a minimum on the potential energy surface. All the calculated vibrational frequencies are scaled by a factor of 0.96[19] to correct the anharmonicity effects.

Materials. All solvents were HPLC grade and used as received. Anhydrous THF and CH_3CN were obtained from the solvent purifier (SPBT-103 of LC Technology Solutions Inc., equipped with a SP-505 column). The moisture content is less than 10 ppm. 2-Methyltetrahydrofuran (MTHF) was dried with sodium metal, and distilled before use. All other solvents and materials for synthesis were reagent grade. The synthesis of both *p*-ABDI[8] and the intermediate (*Z*)-4-bromobenzylidine-2,3-dimethylimidazolinone (*p*-BBDI)[9] has been reported. The target compound *p*-CFABDI was prepared with a palladium-catalyzed C−N coupling reaction between *p*-BBDI and 4-trifluoromethylaniline. The reaction scheme (Scheme S1), synthetic procedures, and data for compound characterization are provided as Supporting Information.

RESULTS AND DISCUSSION

Steady-State Electronic Spectra. The UV−vis absorption and fluorescence spectra of *p*-ABDI and *p*-CFABDI were investigated in hexane, THF, CH_3CN, CH_3OH, and CF_3CH_2OH (trifluoroethanol, TFE). The spectra in CH_3CN are shown in Figure 1, and the corresponding spectral data are summarized in Table 1. Both systems display a single intense absorption band at ~400 nm. The absorption maxima (λ_{abs}) of *p*-CFABDI are red-shifted by ~10 nm from that of *p*-ABDI, attributable to the extended N-arylamino conjugation in *p*-CFABDI.[20] The solvatochromic shift is slightly less for *p*-CFABDI than for *p*-ABDI, because of the electron-withdrawing CF_3 group that weakens the push−pull (charge-transfer) character of *p*-CFABDI. On average, the red shifts are ~950 cm^{-1} when CH_3OH replaces CH_3CN and ~820 cm^{-1} when CH_3CN replaces hexane. As CH_3CN and CH_3OH have comparable polarities, the difference in λ_{abs} could be attributed to SSHB interactions, where CH_3OH serves as HB donor and the solute as HB acceptor. Both the electron-donating anilino nitrogen and the electron-accepting imidazolinone oxygen and nitrogen of *p*-ABDIs are HB acceptors, but their SSHB would

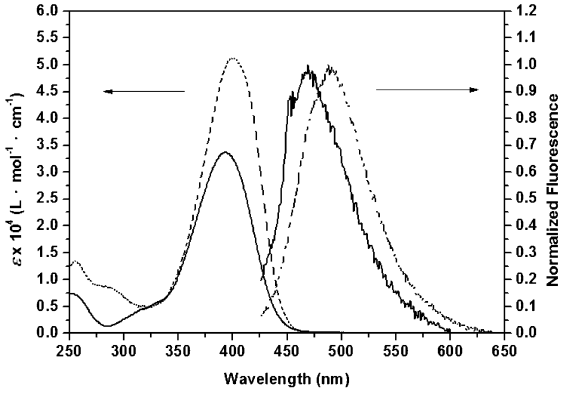

Figure 1. UV−vis absorption and fluorescence spectra of *p*-ABDI (solid) and *p*-CFABDI (dashed) in CH_3CN at 296 K.

Table 1. Maxima of UV−vis Absorption (λ_{abs}) and Fluorescence (λ_f), Absorbance-Band Half-Width ($\Delta\nu_{1/2}$), Quantum Yields for Fluorescence (Φ_f), and $Z \rightarrow E$ Photoisomerization (Φ_{ZE}) for *p*-ABDI and *p*-CFABDI in Protic and Aprotic Solvents at 296 K

compd	solvent	λ_{abs} (nm)	$\Delta\nu_{1/2}$ (cm^{-1})	λ_f (nm)	Φ_f	Φ_{ZE}[a]
p-ABDI	hexane	380	3900	430	$<10^{-3}$	0.45
	THF	397	3900	451	$<10^{-3}$	0.49
	CH_3CN	393	4100	469	$<10^{-3}$	0.50
	CH_3OH	409	4300	481	$<10^{-3}$	0.17
	TFE	386	5300	476	$<10^{-3}$	0.15
p-CFABDI	hexane	390	3800	445	0.002	0.48
	THF	404	3700	466	0.002	0.50
	CH_3CN	402	3900	488	0.002	0.57
	CH_3OH	417	3900	500	0.001	0.48
	TFE	419	4100	514	$<10^{-3}$	0.28

[a]For the purpose of solubility, the hexane, CH_3CN, CH_3OH, and TFE solutions contain 20% THF in measurements of isomerization quantum yields.

dx.doi.org/10.1021/jp3093379 | J. Phys. Chem. B 2013, 117, 2695−2704

impose different effects on λ_{abs}. HB to the donor moiety of chromophores is expected to weaken the push−pull character and thus to decrease the λ_{abs}, and the opposite would be true for HB to the acceptor moiety. That λ_{abs} for CH_3OH is larger than that for CH_3CN indicates that the net electronic perturbation of SSHB with CH_3OH is an enhanced push−pull character for both systems. The situation is different with the stronger HB donor TFE. The λ_{abs} is blue-shifted for *p*-ABDI but red-shifted for *p*-CFABDI on going from CH_3CN or CH_3OH to TFE. This indicates that the net effect of the TFE-solute SSHB is a diminishment for *p*-ABDI but an enhancement for *p*-CFABDI in the push−pull electronic character. Evidently, the electron-withdrawing N-aryl substituent in *p*-CFABDI makes the anilino nitrogen a poor HB acceptor even with TFE. This argument is consistent with the relative size of absorption-band half-width ($\Delta\nu_{1/2}$), which reflects the distribution of specific HB and nonspecific solvating species (Figure S2, Supporting Information). The $\Delta\nu_{1/2}$ is 4000 ± 100 cm^{-1} for *p*-ABDI in the three aprotic solvents, and it increases to 4300 cm^{-1} in CH_3OH and to 5300 cm^{-1} in TFE. In contrast, $\Delta\nu_{1/2}$ is 3800 ± 100 cm^{-1} for *p*-CFABDI in all three aprotic solvents and in CH_3OH, and it increases slightly to 4100 cm^{-1} in TFE.

The electronic nature of *p*-ABDI as compared to *p*-HBDI deserves a discussion. According to the Hammett substituent constants,[21] the amino ($\sigma_{p\text{-}NH_2}$ = −0.66) group in *p*-ABDI is expected to have an electron-donating capacity intermediate between the hydroxyl ($\sigma_{p\text{-}OH}$ = −0.37) and oxido ($\sigma_{p\text{-}O^-}$ = −0.81) groups that correspond to neutral and anionic forms of *p*-HBDI. The observed λ_{abs} of *p*-ABDI indeed lies in between those of neutral and anionic forms of *p*-HBDI in the same solvents.[22] For example, the neutral *p*-HBDI, *p*-ABDI, and anionic *p*-HBDI display λ_{abs} at 365, 397, and 456 nm in THF, at 361, 393, and 452 nm in CH_3CN, and at 367, 409, and 428 nm in CH_3OH, respectively. The difference in λ_{abs} between *p*-ABDI and neutral *p*-HBDI is smaller than that between *p*-ABDI and anionic *p*-HBDI in THF and CH_3CN, but the opposite is true in CH_3OH. By following the same concept of SSHB on λ_{abs} as discussed above, the significant blue shift of anionic *p*-HBDI on going form THF and CH_3CN to CH_3OH is a consequence of weakened push−pull character due to strong SSHB between CH_3OH and the oxido group. The corresponding SSHB effect on λ_{abs} is much weaker in both *p*-ABDI and neutral *p*-HBDI. Therefore, we might conclude that the electronic character of *p*-ABDI resembles that of neutral *p*-HBDI more than that of anionic *p*-HBDI. This conclusion is important for the discussion of the excited-state decay mechanism (vide infra), because recent quantum chemical calculations[4c] indicated that both the φ and τ torsions are possible for anionic *p*-HBDI but only the τ torsion is favorable for the neutral form.

The fluorescence spectra of *p*-ABDI and *p*-CFABDI were investigated in selected solvents at various temperatures (Figures S3 and S4, Supporting Information). We previously reported that the fluorescence of *p*-ABDI is extremely weak in solutions at ambient temperature.[8] Because of larger noises, the reported fluorescence maxima (λ_f) at 296 K must be treated with caution, but the identity of the spectra is justified by the fact that the corresponding excitation spectra (not shown) conform to the absorption spectra. In contrast, the fluorescence of *p*-CFABDI was readily detected at both 298 and 80−160 K. That the fluorescence intensity for *p*-CFABDI is greater than that for *p*-ABDI is a consequence of the amino conjugation effect, which was originally observed for *trans*-aminostilbenes[10] and is valid also for the ABDI systems.[9] This effect with N-arylamino conjugation is interpreted as implying an increased barrier height along the isomerization path. The solvatochromic shifts for λ_f larger than for λ_{abs} indicate an increased molecular dipole in the electronically excited state.

Quantum Yields. The Φ_f and Φ_{ZE} values of *p*-ABDI and *p*-CFABDI in hexane, THF, CH_3CN, CH_3OH, and TFE are reported in Table 1. Compared to *p*-ABDI, *p*-CFABDI exhibits stronger fluorescence in all solvents except TFE with the Φ_f values (0.001−0.002) essentially the same as those reported previously for amino-conjugated analogue *p*-PhABDI (Chart 1).[9] We previously reported that the *E* isomer of *p*-ABDI is relatively stable in solvents such as DMSO and CH_3OH near 296 K, such that the thermal $E \rightarrow Z$ isomerization was unobserved.[8] This condition is true also for the *E* isomer of *p*-CFABDI. The absence of thermal isomerization renders a straightforward determination of Φ_{ZE} with HPLC analysis. Φ_{ZE} is near 0.50 in most cases, but it is only 0.15−0.17 for *p*-ABDI in CH_3OH and TFE and 0.28 for *p*-CFABDI in TFE.

The lower values of Φ_{ZE} in protic vs aprotic solvents indicate that the SSHB interactions perturb the $Z \rightarrow E$ conversion. According to the OBF model for the *Z*,*E*-photoisomerization,[23] the perpendicular (near 90° of the τ torsion) intermediate $^1p^*$ undergoes IC to the ground electronic state ^1p, from which either the *E* or the *Z* isomer is formed. It is reasonable to assume an equal probability for $^1p \rightarrow E$ and for $^1p \rightarrow Z$ because of a similar driving force; the quantum efficiency of the τ torsion can hence be estimated as $2\Phi_{ZE}$. When the nonradiative decay involves mainly the τ torsion, the system displays $\Phi_f + 2\Phi_{ZE} \cong 1.0$. In contrast, a behavior of $\Phi_f + 2\Phi_{ZE} \ll 1.0$ indicates either the presence of other IC channels that compete with the τ torsion or a perturbation of the τ torsion toward $^1p^*$ so that formation of the *E* isomer is diminished. The observation that $\Phi_f + 2\Phi_{ZE} = 0.34$ for *p*-ABDI in CH_3OH was previously attributed to the presence of a SSHB-induced IC channel.[8] However, as indicated by the time-resolved fluorescence and IR spectra (vide infra), the condition that $\Phi_f + 2\Phi_{ZE} \ll 1.0$ for *p*-ABDI and *p*-CFABDI more likely results from a modified PES for the τ torsion so that recovery of the *Z* isomer becomes more favorable.

Steady-State IR Absorption. The ground-state IR spectra in the spectral region 1500−1750 cm^{-1} for *p*-ABDI and *p*-CFABDI in CD_3CN, CH_3OH, and CD_3OD are shown in Figure 2 with normalized maximal absorption near 1600 cm^{-1}. The major absorption lines near 1690, 1635, 1600, and 1520 cm^{-1} for *p*-ABDI were assigned to vibrational modes according to the DFT calculations at the B3LYP/6-31G* level of theory, as listed in Table 2 and depicted in Figure S5 (Supporting Information). The most intense line near 1600 cm^{-1} is assigned to the phenyl stretching mode coupled with the amino NH_2 bending mode. The neighboring lines near 1635 and 1520 cm^{-1} are associated with the NH_2 bending and the phenyl symmetric stretching modes, respectively. The line near 1690 cm^{-1} is associated with the C═O stretching mode. For comparison, the C═O stretching mode of *p*-HBDI in CD_3OD was reported to be 1690−1704 cm^{-1}.[24] The relative intensities of these absorption lines in CD_3CN (Table 2) are consistent with the calculated values. In contrast, absorptions near 1690 and 1635 cm^{-1} are weaker in CH_3OH and CD_3OD than in CD_3CN, indicating that the SSHB induces the structural change in the ground state. The IR spectra of *p*-CFABDI are similar to those of *p*-ABDI in terms of the line positions and relative intensities,

dx.doi.org/10.1021/jp3093379 | J. Phys. Chem. B 2013, 117, 2695−2704

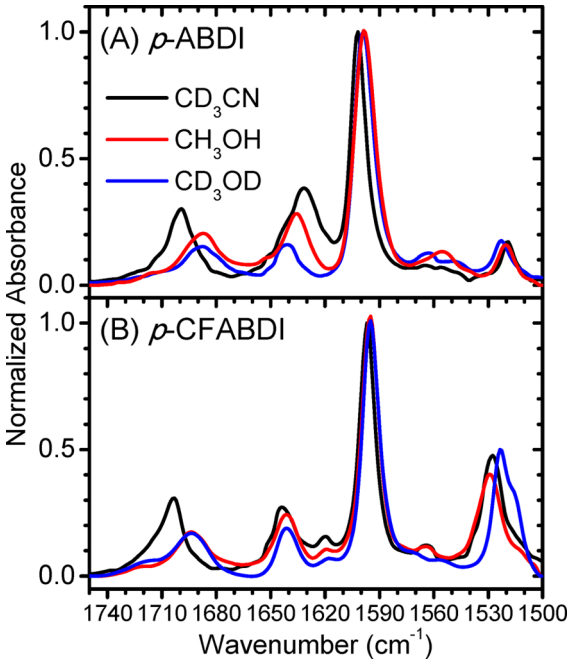

Figure 2. IR spectra in the region 1500−1750 cm^{-1} of (A) *p*-ABDI and (B) *p*-CFABDI in CD_3CN, CH_3OH, and CD_3OD. Absorbance is normalized at ∼1600 cm^{-1}.

except that the line intensity near 1528 cm^{-1} is larger than that of *p*-ABDI. The related vibrational modes for *p*-CFABDI are listed in Table 2 and depicted in Figure S6 (Supporting Information).

Femtosecond fluorescence decays and UV-pump-IR-probe transient absorption spectra have been measured for *p*-ABDI and *p*-CFABDI in CD_3CN, CH_3OH, and CD_3OD. The excitation wavelength is 400 nm, near the absorption maximum of both compounds.

Femtosecond Fluorescence Decays. The fluorescence decays of *p*-ABDI measured at three wavelengths (500, 550, and 600 nm) were all fitted well with biexponential functions (Figure 3). The decays show a subpicosecond component (∼0.3 ps, 39−86%) and a picosecond component (∼1.0 ps, 14−61%) with time constants nearly independent of the solvent and probe wavelength (Table 3). Emission of the subpicosecond component appears to be slightly red-shifted as compared to that of the picosecond component, as the weight of the former is increased at the longer emission wavelengths.

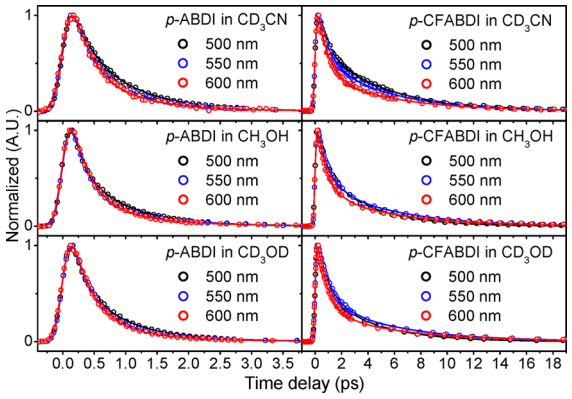

Figure 3. Fluorescence decay profiles for *p*-ABDI and *p*-CFABDI in CD_3CN, CH_3OH, and CD_3OD probed at three selected wavelengths. All data were fitted with a sum of two exponential terms as listed in Table 3.

These ultrafast decays of the lowest singlet excited (S_1) state are consistent with the extremely small fluorescence quantum yields of *p*-ABDI ($\Phi_f < 10^{-3}$) in solutions. A biexponential population decay might arise from two distinct emitting populations or from a Gaussian distribution of decay times associated with a distribution of conformations.[25] The ground state of *p*-ABDI likely exists as a distribution of conformers of different φ torsion angles, and they might encounter different barriers along the τ-torsion coordinate in the excited state. Nevertheless, the rapid fluorescence quenching (0.3−1.0 ps) indicates that the τ-torsion barrier is extremely small.

As is the case of *p*-ABDI, the fluorescence decays of *p*-CFABDI are biphasic in nature, which can be well described by a biexponential decay function for transients probed at all three wavelengths (500, 550, and 600 nm) and in all three solvents (Figure 3). The decay time constants ∼0.8 and ∼5.5 ps probed at 550 and 600 nm are insensitive to the solvent, but that of the longer-time component decreased (3.7−4.0 ps) in CH_3OH and CD_3OD when the probe wavelength was 500 nm (Table 3). The phenomena of increased weights of the short-time component at longer probe wavelengths observed for *p*-ABDI were observed also for *p*-CFABDI. The much slower decays of *p*-CFABDI relative to those of *p*-ABDI are consistent with the larger Φ_f values listed in Table 1, indicating the involvement of a larger energy barrier along the τ-torsion coordinate on the S_1 PES for the former than the latter.

Table 2. Comparison of Observed IR Absorption Lines of *p*-ABDI and *p*-CFABDI in Selected Solvents in the Region 1500−1750 cm^{-1} with Scaled Harmonic Vibrational Wavenumbers

		wavenumber[a] (cm^{-1})				
compd	mode	CD_3CN	CH_3OH	CD_3OD	caln[b]	mode description
p-ABDI	ν_{62}	1519 (8)	1520 (8)	1523 (9)	1504 (13)	phenyl symmetric stretch
	ν_{65}	1601 (100)	1598 (100)	1598 (100)	1598 (100)	phenyl stretch + NH_2 bend
	ν_{66}	1632 (76)	1636 (20)	1641 (10)	1623 (73)	NH_2 bend
	ν_{68}	1700 (39)	1688 (21)	1688 (14)	1726 (50)	C═O stretch
p-CFABDI	ν_{97}	1528 (52)	1529 (58)	1521 (57)	1510 (61)	exocyclic-CNC asymmetric stretch
	ν_{101}	1597 (100)	1595 (100)	1595 (100)	1591 (100)	phenyl stretch
	ν_{103}	1642 (30)	1644 (34)	1641 (17)	1635 (24)	exocyclic C═C stretch + C═N stretch + phenyl stretch
	ν_{104}	1705 (36)	1691 (44)	1695 (26)	1730 (32)	C═O stretch

[a]Relative intensities normalized to the absorption near 1600 cm^{-1} are listed in parentheses. [b]Vibrational wavenumbers calculated with B3LYP/6-31G* are scaled by 0.960.[19]

dx.doi.org/10.1021/jp3093379 | J. Phys. Chem. B 2013, 117, 2695−2704

Table 3. Fluorescence Decay Time Constants (τ_f) and Ground-State Recovery Time Constants (τ_{gr}) of *p*-ABDI and *p*-CFABDI in CD_3CN, CH_3OH, and CD_3OD

		τ_f[a] (ps)			τ_{gr}[b] (ps)	
compd	solvent	500 nm	550 nm	600 nm	maximum	edge
p-ABDI	CD_3CN	0.28 (39)	0.30 (60)	0.31 (71)	18.3 ± 0.8 [1609]	20.9 ± 2.2 [1613]
		0.85 (61)	0.88 (40)	0.90 (29)		
	CH_3OH	0.17 (54)	0.27 (76)	0.29 (81)	7.3 ± 0.1 [1609]	7.5 ± 0.2 [1613]
		0.97 (46)	0.97 (24)	0.97 (19)		
	CD_3OD	0.20 (53)	0.35 (81)	0.35 (86)	9.4 ± 0.3 [1601]	12.1 ± 0.7 [1605]
		0.79 (47)	1.05 (19)	1.08 (14)		
p-CFABDI	CD_3CN	0.82 (41)	0.86 (53)	0.84 (69)	25.4 ± 0.8 [1607]	26.0 ± 1.1 [1609]
		4.95 (59)	5.09 (47)	5.49 (31)		
	CH_3OH	0.70 (48)	0.85 (60)	0.76 (69)	11.3 ± 0.3 [1605]	10.7 ± 0.9 [1611]
		3.67 (52)	5.33 (40)	5.47 (31)		
	CD_3OD	0.76 (52)	0.95 (62)	0.83 (73)	16.0 ± 0.7 [1600]	18.4 ± 1.0 [1605]
		3.96 (48)	5.66 (38)	6.05 (27)		

[a]Relative amplitudes of the exponential decay components are listed in parentheses. [b]Time constants of the recovery of the bleached signal. The exactly probed wavenumber is shown in brackets.

Transient Infrared Spectra. Figure 4 shows the two-dimensional contour plot of the time-resolved infrared (TRIR) difference spectra recorded for *p*-ABDI in the spectral range 1515−1740 cm^{-1} and in the time domains 0−30 ps (CH_3OH), 0−40 ps (CD_3OD), and 0−60 ps (CD_3CN) upon excitation at 400 nm. For comparison, the ground-state spectra in the same spectral region are presented as green traces. The difference spectra recorded at 0.5 ps and the temporal profiles monitored at 1609 cm^{-1} (1601 cm^{-1} for CD_3OD solution) are also shown. The bleached absorption bands (negative signals) near 1635 and 1600 cm^{-1} are shifted toward greater wavenumbers relative to those of the ground-state absorptions in CD_3CN and CH_3OH, but the shifts are less significant in CD_3OD. The shifts are attributed to the superposition of positive absorption at the low-energy side due to absorption of the hot ground electronic state. The assignment of the positive absorptions to a hot ground electronic state rather than an excited state relies on the fact that the positive absorption bands correlate well with those of the ground state and their decay times are comparable to the recovery times of the bleached signals, which are much longer (see below) than the fluorescence decay times (≤1 ps). In addition, it is widely accepted that the τ-twisted dark excited state $^1p^*$ of alkenes such as stilbene is short-lived, within a few hundred femtoseconds.[26] A weaker positive absorption near the bleached signal would result in a smaller shift of the bleached band. For comparison, there is also a small shift toward greater wavenumber (~10 cm^{-1}) for the absorption band near 1600 cm^{-1} from the S_0 to the S_1 state for anionic *p*-HBDI in CD_3OD, but the corresponding shifts for the neutral and cationic forms of *p*-HBDI are negligible.[24] The decay time constants of the bleached signals (or times for the ground-state recovery, τ_{gr}) near 1600 cm^{-1} are highly dependent on the solvent; they are 7.3 ± 0.1, 9.4 ± 0.3, and 18.3 ± 0.8 ps in CH_3OH, CD_3OD, and CD_3CN, respectively. To minimize the interference from the hot ground electronic state, we monitored also the recovery of ground-state *p*-ABDI in CH_3OH, CD_3OD, and CD_3CN, respectively, at 1613, 1605, and 1613 cm^{-1} and obtained time constants of 7.5 ± 0.2, 12.1 ± 0.7, and 20.9 ± 2.2 ps. The absence of explicit contributions of the excited state to the TRIR spectra could be attributed to its short lifetime and weak intensity. According to TDDFT calculations, the major IR absorption bands of *p*-ABDI in its S_1 state are likely overlapped with the bleached bands near 1600 cm^{-1} (Figure S7, Supporting Information).

The time-resolved and ground-state IR spectra of *p*-CFABDI in the region 1515−1740 cm^{-1} are similar to those of *p*-ABDI (Figure 5). Larger wavenumber shifts for the absorptions at 1641 and 1594 cm^{-1} for CD_3CN and CH_3OH than for CD_3OD were also observed. The τ_{gr} of the signals at 1605 cm^{-1} are also highly dependent on the solvent; they are 11.3 ± 0.3, 16.0 ± 0.7, and 25.4 ± 0.8 ps for CH_3OH, CD_3OD, and CD_3CN, respectively. Those monitored at ~10 cm^{-1} greater in wavenumber to avoid interference from the product are 10.7 ± 0.9, 18.4 ± 1.0, and 26.0 ± 1.1 ps for CH_3OH, CD_3OD, and CD_3CN, respectively. These values are listed in Table 3 for comparison.

Excited-State Relaxation Mechanism. Whether the τ or the φ torsion is responsible for the IC of *p*-HBDI has been extensively discussed in the literature.[2−6] In the following discussion, several pieces of evidence have driven us to conclude that the τ torsion plays the major, if not the only, role in accounting for the nonradiative deactivation of *p*-ABDI and *p*-CFABDI in solutions.

First, as indicated by the λ_{abs} values, the push−pull electronic character of *p*-ABDI is between that of neutral and anionic *p*-HBDI, but it resembles neutral *p*-HBDI more than anionic *p*-HBDI. For *p*-ABDI, the charge-transfer resonance structure corresponds to the anionic form of *p*-HBDI (Figure 6a and b). It appears that this charged resonance form plays a minor role in the electronic nature of *p*-ABDI. Recent quantum chemical calculations reported by Olsen et al. suggested that the φ-torsion-induced IC is possible only for the anionic form but not for the neutral form of the GFP chromophore.[4c] According to this concept, the large deviation of *p*-ABDI from the anionic *p*-HBDI would not favor the φ torsion in the excited-state deactivation. As the electron-donating power of the amino group in *p*-CFABDI is even lower than that in *p*-ABDI, the relative importance of the charge-transfer resonance form would be further diminished and so is the possibility of the φ torsion.

Second, the results that $\Phi_f + 2\Phi_{ZE} \cong 1.0$ for both *p*-ABDI and *p*-CFABDI in CH_3CN is a strong indication that the τ torsion is responsible for the IC of both systems and that the decay dynamics follow a conventional OBF mechanism of *Z*−*E* photoisomerization (the solid line in Figure 7),[27] as seen for

dx.doi.org/10.1021/jp3093379 | J. Phys. Chem. B 2013, 117, 2695−2704

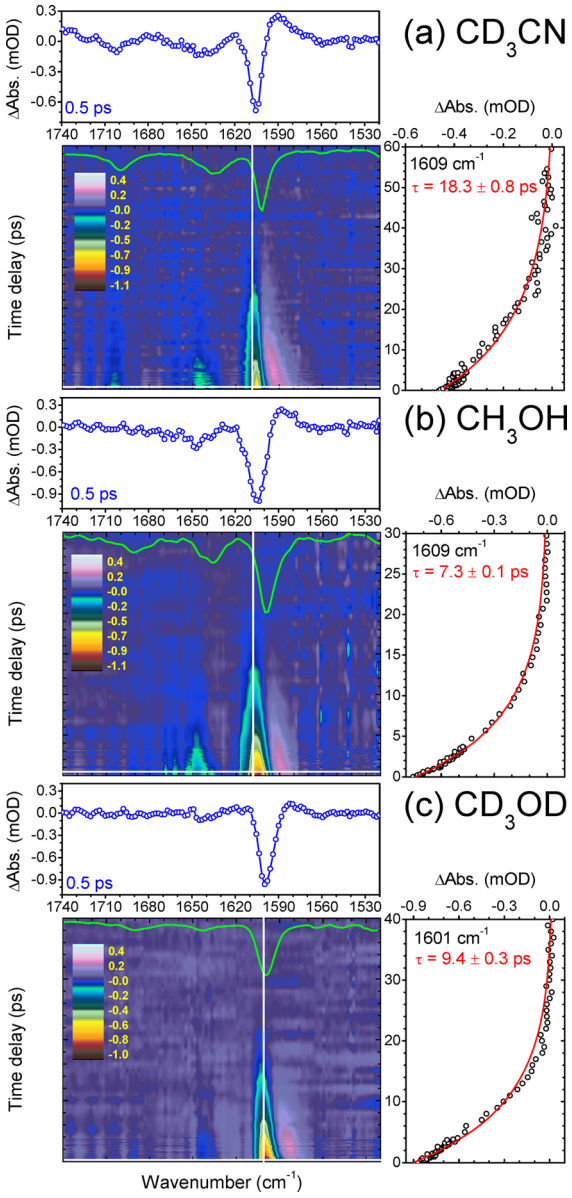

Figure 4. Two-dimensional frequency–time TRIR spectra of *p*-ABDI in (a) CD_3CN, (b) CH_3OH, and (c) CD_3OD upon 400 nm excitation. The absorption spectra (green) of the ground state are present for comparison. Upper figures are the TRIR spectra recorded at 0.5 ps, and right figures are the temporal profiles monitored at the maximum of the bleached signal near 1600 cm^{-1}.

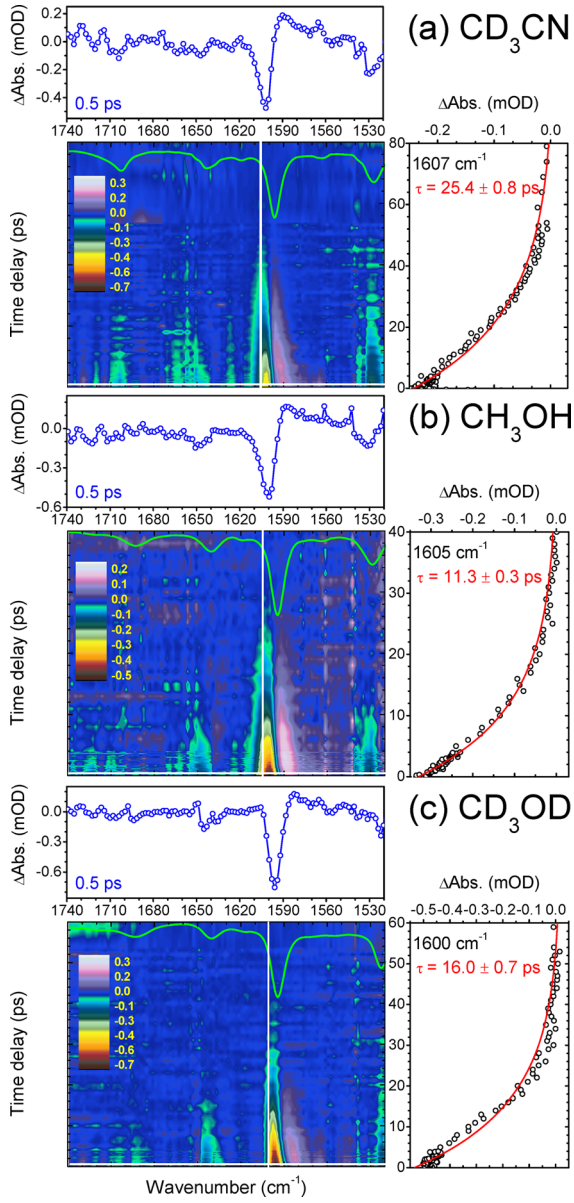

Figure 5. Two-dimensional frequency–time TRIR spectra of *p*-CFABDI in (a) CD_3CN, (b) CH_3OH, and (c) CD_3OD upon 400 nm excitation. The absorption spectra (green) of the ground state are present for comparison. Upper figures are the TRIR spectra recorded at 0.5 ps, and right figures are the temporal profiles monitored at the maximum of the bleached signal near 1600 cm^{-1}.

both the parent and push–pull stilbenes.[10,12,28,29] According to the scenario of τ torsion-induced fluorescence quenching, the longer decay times for *p*-CFABDI vs *p*-ABDI indicate a larger torsional barrier in the S_1 excited state for *p*-CFABDI. The smaller rates of the τ torsion for *p*-CFABDI vs *p*-ABDI account also for the larger fluorescence quantum efficiency. Examples of fluorescence enhancement due to increased τ-torsion barrier have been demonstrated, including N-aryl substitution of *trans*-aminostilbenes.[10] We have recently shown that this N-arylamino-enhanced fluorescence effect is observed also for *p*-ABDI.[9] Compound *p*-CFABDI is a new addition to the family of N-aryl substituted *p*-ABDIs.

Third, a distribution of conformers due to small φ torsion angles can be expected for GFP chromophores in the ground state, which accounts for their nonexponential fluorescence decay behavior. A recent report by Meech et al. with modified *p*-HBDI chromophores showed that the φ pretwisted species display blue-shifted absorption and fluorescence spectra as compared to the planar chromophores.[30] If the φ torsion was responsible for the IC of *p*-ABDI (i.e., the presence of a φ-twisted dark excited state), we would have expected a faster fluorescence quenching for the φ pretwisted conformers than the planar conformers, and the short-time component would emit at shorter wavelengths. In contrast, with the τ-torsion IC mechanism, the φ pretwisted conformers might undergo structural planarization before the τ torsion, and thus their fluorescence lifetimes would be longer than conformers of near planarity. This predicts a larger weight at the shorter probed wavelengths for the longer-time component. The observed

dx.doi.org/10.1021/jp3093379 | J. Phys. Chem. B 2013, 117, 2695–2704

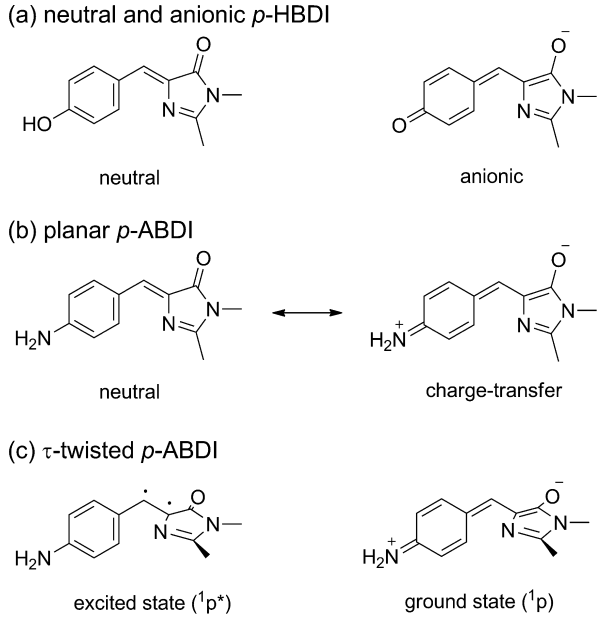

Figure 6. (a) Neutral and anionic *p*-HBDI, (b) two-state resonance structure of *p*-ABDI, and (c) the ground- and excited-state structures of *p*-ABDI at a τ angle of 90°, corresponding to the ^{1}p and ^{1}p* states in Figure 7.

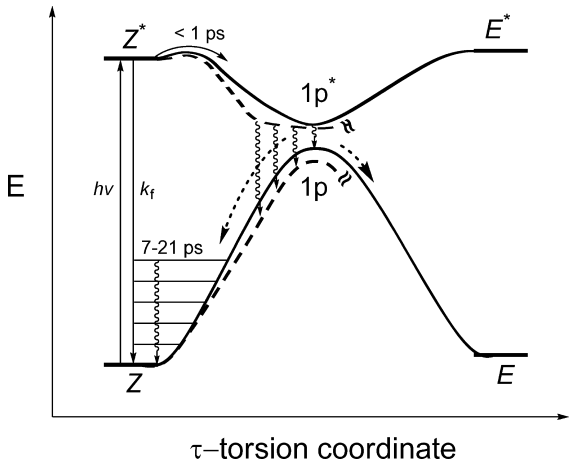

Figure 7. Simplified scheme for the proposed potential energy surfaces along the τ-torsion coordinate for the excited state of *p*-ABDI in aprotic CH_3CN (solid curve) and protic CH_3OH (dashed curve) solvents. The dashed arrows represent the partition of the τ-twisted intermediates to the *E* (minor) and *Z* (major) isomers in CH_3OH.

fluorescence decay behavior is again consistent with the τ torsion mechanism.

Finally, although the Φ_{ZE} is diminished for *p*-ABDI and *p*-CFABDI in CH_3OH and/or TFE, the possibility of SSHB-induced IC[31] through the φ torsion or solvent-to-substrate ESPT that competes with the τ torsion is inconsistent with the solvent-independent femtosecond fluorescence decay and the absence of new absorption features in the transient IR absorption spectra. An alternative explanation of the SSHB effect on Φ_{ZE} is a perturbation of the PES along the τ torsion by SSHB in a way that IC takes place not only at ^{1}p* but also at smaller τ torsional angles (Figure 7). Whereas an equal partition to the *E* vs *Z* isomer is expected for the IC at ^{1}p* (τ-torsion angle 90°), the IC at a τ-torsion angle smaller than 90° would energetically favor a recovery of the *Z* isomer (i.e., aborted isomerization). To rationalize an effective and competitive IC for the τ-twisted intermediates before reaching an angle of 90° (e.g., ^{1}p*), a shallow PES near ^{1}p* is proposed. It is anticipated that the charge-transfer character of the excited *p*-ABDI is significant at the onset (i.e., *Z**) along the τ-torsion coordinate, because this resonance form has a single-bond character for the τ torsion. However, according to the quantum chemical three-state model developed by Olsen and McKenzie,[32] the charge-transfer character is reduced at ^{1}p* but enhanced at ^{1}p (Figure 6c). It is conceivable that some of the SSHB modes, particularly those associated with the imidazolinone carbonyl group,[25,33] lower the energy of the excited-state PES at the earlier stage of the τ torsion and that of the ground-state PES near ^{1}p (the dashed curves in Figure 7). Therefore, the probability of IC is increased at τ angles smaller than 90° but decreased at τ = 90° in CH_3OH vs CH_3CN. This model explains also the smaller SSHB effect on the Φ_{ZE} of *p*-CFABDI vs *p*-ABDI, as the charge-transfer character of *p*-CFABDI is weaker than that of *p*-ABDI. A large modification of the excited-state PES along the τ torsion coordinate by SSHB is also observed for the *meta* isomer *m*-ABDI.[34]

The dependence of the rates of the ground-state recovery on solvent proticity is attributed to vibrational cooling of the hot ground state formed after IC of the τ-twisted species. The τ_{gr} values 7.3 ± 0.1 and 18.3 ± 0.8 ps observed for *p*-ABDI in CH_3OH and CD_3CN, respectively, are within the typical vibrational cooling time scales (tens of picoseconds) of the hot ground electronic state.[35] For comparison, the cooling times of *p*-HBDI in CH_3OH and CH_3CN are 4.8 ± 0.5 and 13.0 ± 0.5 ps, respectively,[5b] and those of *trans*-stilbene in CH_3OH and cyclohexane are 17 ± 5 and 39 ± 10 ps, respectively.[35a] The faster ground-state recovery for *p*-ABDI vs *trans*-stilbene in CH_3OH and for *p*-ABDI in CH_3OH vs CD_3CN is also consistent with the expectation that it takes less time to become the planar *p*-ABDI in its ground electronic state if IC takes place at a τ-torsion angle smaller than 90°. The different τ_{gr} in CH_3OH (7.3 ± 0.1 ps) vs CD_3OD (9.4 ± 0.3 ps) highlights the solvent isotope effect on the cooling dynamics.

CONCLUSION

According to the quantum yields for isomerization, fluorescence decay time constants, and TRIR data, we conclude that the nonradiative decay of *p*-ABDI and *p*-CFABDI is governed by the τ torsion in both aprotic and protic solvents, but in protic solvents, such as CH_3OH, the SSHB interactions perturb the PES for the τ torsion in a way that the IC occurs at a distribution of τ-torsion angles smaller than 90°. Consequently, the SSHB diminishes the quantum yields for the $Z \rightarrow E$ isomerization but has a negligible influence on the fluorescence quenching kinetics. The IC results in a hot ground electronic state that exhibits solvent-dependent cooling dynamics. As the phenomena of Φ_{ZE} dependent on solvent proticity and ultrafast quenching of fluorescence followed by slower recovery of the ground state have also been observed for the GFP chromophore *p*-HBDI,[8,24] the excited-state dynamics elucidated herein for *p*-ABDI might provide insights into the photophysics of *p*-HBDI in solution.

ASSOCIATED CONTENT

Supporting Information

Detailed synthetic scheme, procedures, and characterization data for *p*-CFABDI, absorption and fluorescence spectra, temperature dependence of fluorescence spectra between 80

dx.doi.org/10.1021/jp3093379 | J. Phys. Chem. B 2013, 117, 2695−2704

and 160 K, displacement vectors of the vibration modes listed in Table 2, complete ref 17, and DFT calculated coordinates. This material is available free of charge via the Internet at http://pubs.acs.org.

AUTHOR INFORMATION

Corresponding Author

*Phone: (+886)35131459 (Y.-P.L.); (+886)35131524 (E.W.-G.D.); (+886)233661649 (J.-S.Y.). E-mail: yplee@mail.nctu.edu.tw (Y.-P.L.); diau@mail.nctu.edu.tw (E.W.-G.D.); jsyang@ntu.edu.tw (J.-S.Y.).

Notes

The authors declare no competing financial interest.

ACKNOWLEDGMENTS

National Science Council of Taiwan (Grant Nos. NSC100-2745-M-009-001-ASP and NSC98-2119-M-002-008-MY3) and the Ministry of Education, Taiwan ("Aim for the Top University Plan" of NCTU and the Excellent Research Project 10R80912-3 of NTU) supported this work. The National Center for High-Performance Computing and the Computing Center of NTU provided computer time. We thank Dr. Chao-Ping Hsu at the Institute of Chemistry of Academia Sinica for helpful discussions.

REFERENCES

(1) (a) Tsien, R. Y. The Green Fluorescent Protein. *Annu. Rev. Biochem.* **1998**, *67*, 509−544. (b) Zimmer, M. Green Fluorescent Protein (GFP): Applications, Structure, and Related Photophysical Behavior. *Chem. Rev.* **2002**, *102*, 759−782. (c) Frommer, W. B.; Davidson, M. W.; Campbell, R. E. Genetically Encoded Biosensors Based on Engineered Fluorescent Proteins. *Chem. Soc. Rev.* **2009**, *38*, 2833−2841. (d) Day, R. N.; Davidson, M. W. The Fluorescent Protein Palette: Tools for Cellular Imaging. *Chem. Soc. Rev.* **2009**, *38*, 2887−2921. (e) Remington, S. J. Green Fluorescent Protein: A perspective. *Protein Sci.* **2011**, *20*, 1509−1519.

(2) Niwa, H.; Inouye, S.; Hirano, T.; Matsuno, T.; Kojima, S.; Kubota, M.; Ohashi, M.; Tsuji, F. I. Chemical Nature of the Light Emitter of the Aequorea Green Fluorescent Protein. *Proc. Natl. Acad. Sci. U.S.A.* **1996**, *93*, 13617−13622.

(3) (a) Meech, S. R. Excited State Reactions in Fluorescent Proteins. *Chem. Soc. Rev.* **2009**, *38*, 2922−2934. (b) Tolbert, L. M.; Baldridge, A.; Kowalik, J.; Solntsev, K. M. Collapse and Recovery of Green Fluorescent Protein Chromophore Emission through Topological Effects. *Acc. Chem. Res.* **2012**, *45*, 171−181.

(4) (a) Martin, M. E.; Negri, F.; Olivucci, M. Origin, Nature, and Fate of the Fluorescent State of the Green Fluorescent Protein Chromophore at the CASPT2//CASSCF Resolution. *J. Am. Chem. Soc.* **2004**, *126*, 5452−5464. (b) Olsen, S.; Smith, S. C. Bond Selection in the Photoisomerization Reaction of Anionic Green Fluorescent Protein and Kindling Fluorescent Protein Chromophore Models. *J. Am. Chem. Soc.* **2008**, *130*, 8677−8689. (c) Olsen, S.; Lamothe, K.; Martínez, T. J. Protonic Gating of Excited-State Twisting and Charge Localization in GFP Chromophores: A Mechanistic Hypothesis for Reversible Photoswitching. *J. Am. Chem. Soc.* **2010**, *132*, 1192−1193.

(5) (a) Stavrov, S. S.; Solntsev, K. M.; Tolbert, L. M.; Huppert, D. Probing the Decay Coordinate of the Green Fluorescent Protein: Arrest of *cis-trans* Isomerization by the Protein Significantly Narrows the Fluorescence Spectra. *J. Am. Chem. Soc.* **2006**, *128*, 1540−1546. (b) Solntsev, K. M.; Poizat, O.; Dong, J.; Rehault, J.; Lou, Y.; Burda, C.; Tolbert, L. M. *Meta* and *para* Effects in the Ultrafast Excited-State Dynamics of the Green Fluorescent Protein Chromophores. *J. Phys. Chem. B* **2008**, *112*, 2700−2711.

(6) Chen, M. C.; Lambert, C. R.; Urgitis, J. D.; Zimmer, M. Photoisomerization of Green Fluorescent Protein and the Dimensions of the Chromophore Cavity. *Chem. Phys.* **2001**, *270*, 157−164.

(7) Webber, N. M.; Litvinenko, K. L.; Meech, S. R. Radiationless Relaxation in a Synthetic Analogue of the Green Fluorescent Protein Chromophore. *J. Phys. Chem. B* **2001**, *105*, 8036−8039.

(8) Yang, J.-S.; Huang, G.-J.; Liu, Y.-H.; Peng, S.-M. Photoisomerization of the Green Fluorescence Protein Chromophore and the *meta*- and *para*-Amino Analogues. *Chem. Commun.* **2008**, 1344−1346.

(9) Huang, G.-J.; Yang, J.-S. The *N*-Arylamino Conjugation Effect in the Photochemistry of Fluorescent Protein Chromophores and Aminostilbenes. *Chem.—Asian J.* **2010**, *5*, 2075−2085.

(10) Yang, J.-S.; Chiou, S.-Y.; Liau, K.-L. Fluorescence Enhancement of *trans*-4-Aminostilbene by *N*-Phenyl Substitutions: the "Amino Conjugation Effect". *J. Am. Chem. Soc.* **2002**, *124*, 2518−2527.

(11) (a) Rettig, W. Charge Separation in Excited States of Decoupled Systems—TICT Compounds and Implications Regarding the Development of New Laser Dyes and the Primary Process of Vision and Photosynthesis. *Angew. Chem., Int. Ed. Engl.* **1986**, *25*, 971−988. (b) Grabowski, Z. R.; Rotkiewicz, K. Structural Changes Accompanying Intramolecular Electron Transfer: Focus on Twisted Intramolecular Charge-Transfer States and Structures. *Chem. Rev.* **2003**, *103*, 3899−4031.

(12) Yang, J.-S.; Liau, K.-L.; Wang, C.-M.; Hwang, C.-Y. Substituent-Dependent Photoinduced Intramolecular Charge Transfer in *N*-aryl-Substituted *trans*-4-Aminostilbenes. *J. Am. Chem. Soc.* **2004**, *126*, 12325−12335.

(13) Dawson, W. R.; Windsor, M. W. Fluorescence Yields of Aromatic Compounds. *J. Phys. Chem.* **1968**, *72*, 3251−3260.

(14) Kubin, R. F.; Fletcher, A. N. Fluorescence Quantum Yields of Some Rhodamine dyes. *J. Lumin.* **1982**, *27*, 455−462.

(15) Luo, L.; Lo, C.-F.; Lin, C.-Y.; Chang, I. J.; Diau, E. W.-G. Femtosecond Fluorescence Dynamics of Porphyrin in Solution and Solid Films: The Effects of Aggregation and Interfacial Electron Transfer between Porphyrin and TiO_2. *J. Phys. Chem. B* **2006**, *110*, 410−419.

(16) Chang, C.-W.; Chou, C. K.; Chang, I. J.; Lee, Y.-P.; Diau, E. W.-G. Relaxation Dynamics of Ruthenium Complexes in Solution, PMMA and TiO_2 Films: The Roles of Self-Quenching and Interfacial Electron Transfer. *J. Phys. Chem. C* **2007**, *111*, 13288−13296.

(17) Frisch, M. J.; Trucks, G. W.; Schlegel, H. B.; Scuseria, G. E.; Robb, M. A.; Cheeseman, J. R.; Scalmani, G.; Barone, V.; Mennucci, B.; Petersson, G. A.; et al. *Gaussian 09*; Gaussian, Inc.: Wallingford, CT, 2009.

(18) (a) Becke, A. D. Density-Functional Thermochemistry. III. The Role of Exact Exchange. *J. Chem. Phys.* **1993**, *98*, 5648−5652. (b) Lee, C.; Yang, W.; Parr, R. G. Organic Dyes Containing 1H-Phenanthro-[9,10-d]imidazole Conjugation for Solar Cells. *Phys. Rev. B* **1988**, *37*, 785−789.

(19) (a) Foresman, J. B.; Frisch, Æ. *Exploring Chemistry with Electronic Structure Methods*, 2nd ed.; Gaussian, Inc.: Pittsburgh, PA, 1996. (b) Scott, A. P.; Radom, L. Harmonic Vibrational Frequencies: An Evaluation of Hartree−Fock, Møller−Plesset, Quadratic Configuration Interaction, Density Functional Theory, and Semiempirical Scale Factors. *J. Phys. Chem.* **1996**, *100*, 16502−16513. (c) Andersson, M. P.; Uvdal, P. New Scale Factors for Harmonic Vibrational Frequencies Using the B3LYP Density Functional Method with the Triple-ζ Basis Set 6-311+G(d,p). *J. Phys. Chem. A* **2005**, *109*, 2937−2941.

(20) (a) The N-arylamino conjugation effect on λ_{abs} depends on the electronic nature of the N-aryl group and the electron-pulling moiety of the push−pull chromophore. Our previous studies[10,12,20b] on *trans*-aminostilbenes showed that reducing the electron-donating power of the N-arylamino group or increasing the electron-pulling moiety of the chromophore would reduce the "conjugation effect" of the N-aryl group on red-shifting λ_{abs}. For comparison, *trans*-4-aminostilbene and *trans*-4-(*N*-phenylamino)stilbene display λ_{abs} at 316 and 346 nm in hexane, respectively, giving rise to a red shift of 30 nm for the N-phenyl conjugation effect.[10] As *N*-(4-trifluoromethylphenyl)amino is a weaker donor than *N*-phenylamino and methineimidazolinone is a stronger electron-pulling group than styrene, the N-aryl conjugation

effect of *p*-CFABDI is as expected to be smaller than 30 nm. (b) Yang, J.-S.; Liau, K.-L.; Hwang, C.-Y.; Wang, C.-M. Photoinduced Single-Versus Double-Bond Torsion in Donor-Acceptor-Substituted *trans*-Stilbenes. *J. Phys. Chem. A* **2006**, *110*, 8003−8010.
(21) Hansch, C.; Leo, A.; Taft, R. W. A Survey of Hammett Substituent Constants and Resonance and Field Parameters. *Chem. Rev.* **1991**, *91*, 165−195.
(22) Dong, J.; Solntsev, K. M.; Tolbert, L. M. Solvatochromism of the Green Fluorescence Protein Chromophore and Its Derivatives. *J. Am. Chem. Soc.* **2006**, *128*, 12038−12039.
(23) Zimmer, M. In *Cis-trans Isomerization in Biochemistry*; Dugave, C., Ed.; Wiley-VCH: Weinheim, Germany, 2006; p 77.
(24) Usman, A.; Mohammed, O. F.; Nibbering, E. T. J.; Dong, J.; Solntsev, K. M.; Tolbert, L. M. Excited-State Structure Determination of the Green Fluorescent Protein Chromophore. *J. Am. Chem. Soc.* **2005**, *127*, 11214−11215.
(25) Petkova, I.; Dobrikov, G.; Banerji, N.; Duvanel, G.; Perez, R.; Dimitrov, V.; Nikolov, P.; Vauthey, E. Tuning the Excited-State Dynamics of GFP-Inspired Imidazolone Derivatives. *J. Phys. Chem. A* **2010**, *114*, 10−20.
(26) Saltiel, J.; Waller, A. S.; Sears, D. F., Jr. The Temperature and Medium Dependencies of *cis*-Stilbene Fluorescence. The Energetics of Twisting in the Lowest Excited Singlet State. *J. Am. Chem. Soc.* **1993**, *115*, 2453−2465 and references cited therein.
(27) Rafiq, S.; Rajbongshi, B. K.; Nair, N. N.; Sen, P.; Ramanathan, G. Excited State Relaxation Dynamics of Model Green Fluorescent Protein Chromophore Analogs: Evidence for *cis*−*trans* Isomerism. *J. Phys. Chem. A* **2011**, *115*, 13733−13742.
(28) (a) Saltiel, J.; Sun, Y.-P. In *Photochromism, Molecules and Systems*; Dürr, H., Bouas-Laurent, H., Eds.; Elsevier: Amsterdam, The Netherlands, 1990; pp 64−164. (b) Todd, D. C.; Jean, J. M.; Rosenthal, S. J.; Ruggiero, A. J.; Yang, D.; Fleming, G. R. Fluorescence Upconversion Study of *cis*-Stilbene Isomerization. *J. Chem. Phys.* **1990**, *93*, 8658−8668. (c) Waldeck, D. H. Photoisomerization Dynamics of Stilbenes. *Chem. Rev.* **1991**, *91*, 415−436.
(29) (a) Görner, H.; Kuhn, H. J. *Cis-trans* Photoisomerization of Stilbenes and Stilbene-Like Molecule. *Adv. Photochem.* **1995**, *19*, 1−117. (b) Lewis, F. D.; Kalgutkar, R. S.; Yang, J.-S. The Photochemistry of *trans-ortho-*, *-meta-*, and *-para*-Aminostilbenes. *J. Am. Chem. Soc.* **1999**, *121*, 12045−12053.
(30) Conyard, J.; Kondo, M.; Heisler, I. A.; Jones, G.; Baldridge, A.; Tolbert, L. M.; Solntsev, K. M.; Meech, S. R. Chemically Modulating the Photophysics of the GFP Chromophore. *J. Phys. Chem. B* **2011**, *115*, 1571−1577.
(31) (a) Rajbongshi, B. K.; Sen, P.; Ramanathan, G. Twisted Intramolecular Charge Transfer in a Model Green Fluorescent Protein Luminophore Analog. *Chem. Phys. Lett.* **2010**, *494*, 295−300. (b) Zhao, G.-J.; Han, K.-L. Hydrogen Bonding in the Electronic Excited State. *Acc. Chem. Res.* **2012**, *45*, 404−413.
(32) Olsen, S.; McKenzie, R. H. A Diabatic Three-State Representation of Photoisomerization in the Green Fluorescent Protein Chromophore. *J. Chem. Phys.* **2009**, *130*, 184302−184313.
(33) Huang, G.-J.; Ho, J.-H.; Prabhakar, Ch.; Liu, Y.-H.; Peng, S.-M.; Yang, J.-S. Site-Selective Hydrogen-Bonding-Induced Fluorescence Quenching of Highly Solvatofluorochromic GFP-like Chromophores. *Org. Lett.* **2012**, *14*, 5034−5037.
(34) Cheng, C.-W.; Huang, G.-J.; Hsu, H.-Y.; Prabhakar, Ch.; Lee, Y.-P.; Diau, E. W.-G.; Yang, J.-S. Effects of Hydrogen Bonding on Internal Conversion of GFP-like Chromophores. II. The *meta*-Amino System. *J. Phys. Chem. B* **2013**, DOI: 10.1021/jp3093397.
(35) (a) Phillips, D. L.; Rodier, J.-M.; Myers, A. B. *Cis*-stilbene Photochemistry: Direct Observation of Product Formation and Relaxation through Two-Color UV Pump-Probe Raman Spectroscopy. *Chem. Phys.* **1993**, *175*, 1−12. (b) Hamm, P.; Ohline, S. M.; Zinth, W. Vibrational Cooling after Ultrafast Photoisomerization of Azobenzene Measured by Femtosecond Infrared Spectroscopy. *J. Chem. Phys.* **1997**, *106*, 519−529.